Cell & Bioscience

RESEARCH

Open Access

# *FRRS1L* variants and ferriheme overload drive hyperpigmentation and systemic Iron overload in lanping black bone sheep

Deping Han[1,2†], Yuanyuan Zhang[1,3†], Weidong Deng[4], Xue Yang[1], Jianfei Chen[1], Guoying Hua[1], Hesham Y.A. Darwish[1], Huaming Mao[4], Xiao Gou[4], Jiankui Wang[1], Kai Cui[1], Yuhao Ma[1], Yurong Tai[1], Xianggui Dong[1], Yanzhu Yao[1], Zu Yang[1], Suying Cao[5], Zhengquan Yu[1], Wansheng Liu[3*] and Xuemei Deng[1*]

## Abstract

**Background** Hemoglobin metabolism disorder can result in systemic iron overload, leading to pigmentation in multiple organs. Although these disorders are often of genetic origin, the specific genes and mechanisms remain incompletely understood. Lanping black bone sheep (LP–BBS), a unique population from the high altitudes along the Hengduan Mountains in Yunnan province, exhibits hyperpigmentation in multiple tissues. Investigating the genetic and environmental factors underlying this phenotype provides a natural model to better understand hemoglobin metabolism disorder.

**Results** LP-BBS were found to exhibit increased red blood cell counts, elevated hemoglobin levels, and systemic iron overload, evidenced by hyperpigmentation in various tissues. Histological and molecular analyses revealed that hyperpigmentation is driven by ferriheme overload, an inheritable quantitative trait influenced by both genetic variation and environmental factors. Genome-wide association studies identified *FRRS1L* as a candidate gene, with significant mutations in its 3′-untranslated region (3′-UTR) reducing *FRRS1L* expression. Functional assays demonstrated that insufficient *FRRS1L* expression promotes ferriheme accumulation in reticuloendothelial cells and macrophages, as confirmed in vitro using *FRRS1L* knockdown models. Ferriheme overload was associated with oxidative stress and systemic inflammation, causing pathological damage to critical organs such as the kidney, liver, and uterus.

**Conclusion** This study identifies *FRRS1L* as a key contributor to ferriheme overload through aberrant hemoglobin metabolism in LP–BBS. These findings offer new insights into the genetic basis and pathological mechanisms of iron overload disorders, providing a potential target for therapeutic intervention. Moreover, LP–BBS serves as a valuable natural model for studying hematogenous pigment disorders and their interplay with environmental factors.

†Deping Han and Yuanyuan Zhang contributed equally to this work.

*Correspondence:
Wansheng Liu
wul12@psu.edu
Xuemei Deng
deng@cau.edu.cn

Full list of author information is available at the end of the article

**Keywords** Black bone sheep, Hyperpigmentation, Iron overload, Macrophage, Systemic inflammation

## Background

In humans and other vertebrates, physiological pigmentation is primarily related to melanocytes, which generate different proportions of eumelanin and phaeomelanin, resulting in various skin, hair, and feather colors [1]. Besides the melanin system, other key pigment systems include protoporphyrin, heme, bilirubin, and biliverdin, which are closely related to erythropoiesis, myoglobin, and different bird eggshell colors [2–5]. Disturbances in heme metabolism in humans, resulting in aberrant ferric iron reduction, can lead to various diseases resulting in hyperpigmentation, such as systemic iron overload, methemoglobinemia, purpura, and malarial pigmentation [6–8]. In addition, hyperpigmentation can be associated with drug metabolism and metal overload, such as silver [9, 10].

Hyperpigmentation in animals is rarely reported, with the black bone chicken, also known as the Silky Fowl, being the only known natural vertebrate model characterized by visceral melanin deposition [11, 12]. In 2001, a natural population of domesticated sheep exhibiting hyperpigmentation in internal organs was discovered in Lanping County, Yunnan Province, China [13], and named Lanping–black bone sheep (LP–BBS). While researchers initially hypothesized that the hyperpigmentation in LP–BBS was caused by a mechanism similar to that of the Silky Fowl [13, 14], no definitive genetic evidence linking it to melanogenesis has been identified. LP–BBS is native to the region of the Three Parallel Rivers of the Jinsha, Lancang, and Nujiang Rivers along the Hengduan Mountains (HDMs), a hotspot for speciation and biodiversity [15]. Through selective breeding, a population of LP–BBS with heritable hyperpigmentation traits resembling those of human hemochromatosis has been established.

In humans, hemochromatosis is a genetic condition characterized by systemic iron overload of genetic origin, leading to increased total body iron stores and resultant end-organ damage [16]. The disorder is often caused by homozygous mutations, most commonly the *C282Y* mutation in the homeostatic iron regulator (*HFE*) gene, which regulates iron absorption by modulating the interaction between the transferrin receptor and transferrin [17]. Additional mutations linked to hemochromatosis occur in hepcidin antimicrobial peptide (*HAMP*), hemojuvelin BMP co-receptor (*HJV*, also known as *HFE2*), and transferrin receptor 2 (*TFR2*) [18–20].

Ferroportin (*FPN1*), a cell membrane protein responsible for exporting iron from duodenal epithelial cells, can also contribute to hemochromatosis when mutations prevent hepcidin–ferroportin binding, resulting in hemochromatosis type 4 [20, 21]. Cellular iron overload in hemochromatosis arises from elevated plasma iron concentrations, leading to iron accumulation in parenchymal cells, particularly the liver (hepatocytes), pancreas (pancreatic cells), and heart (cardiomyocytes) [17]. Patients with hemochromatosis are often asymptomatic for many years and, with symptoms in *HFE*-related cases typically emerging between 30 and 40 years of age and affecting multiple organ systems upon manifestation [17].

Despite advances in diagnosing, managing, and treating hemochromatosis, some cases of iron overload can not be attributed to known gene mutations. Furthermore, diagnostic and treatment approaches are sometimes ineffective due to incomplete understanding of disease. For instance, elevated serum ferritin levels can occur in conditions such as nonalcoholic fatty liver disease and alcoholic liver disease, complicating diagnosis [22].

Similar to human hemochromatosis, LP–BBS display dark-colored blood and a pronounced hyperpigmentation phenotype that typically appears around one year of age. However, unlike the mutations in *HFE*, *HAMP*, *HFE2*, *TFR2*, and *FPN1* observed in humans, no mutations in these genes have been identified in the genome of LP–BBS.

To better understand the chemical nature of the pigment and the genetic mechanisms underlying hyperpigmentation in LP–BBS, this study employed genomic and transcriptome analyses to identify single nucleotide polymorphisms (SNPs) and key genes strongly associated with pigment morphogenesis and deposition in LP–BBS. The role of the candidate gene in pigment overload was confirmed through in vitro reproduction of the phenotype. Our findings reveal the origin of pigment and the genetic mechanism responsible for pigment overload in LP–BBS, establishing this population as a valuable mammalian model for investigating the causes and potential treatment of iron-overload diseases in humans.

## Results

### Ferriheme overload contributes to hyperpigmentation in LP–BBS

Hyperpigmentation in Lanping black-bone sheep (LP–BBS) has been a notable phenotype, but its underlying cause remains unclear. Initial hypotheses pointed to melanin as the primary contributor [13]; however, our analysis of tyrosinase, S-100, and MITF revealed that the pigmented tissues lack melanocytes (Additional File 1: Fig. S1A–C). Classical melanocytes with long dendrites were only observed in the dermis of LP–BBS (Additional File 1: Fig. S1D). Key genes associated with melanin synthesis including tyrosinase (*TYR*), melanocortin

1 receptor (*MC1R*) and agouti were not differentially detected between LP–BBS and Lanping non-black bone sheep (LP–NBS) (Additional File 1: Fig. S1E). Furthermore, the pigment in LP–BBS showed no similar absorption peak to the melanin from cuttlefish (using standard control) and Silky Fowl (Additional File 1: Fig. S1F). Other pigment hemosiderin, lipofuscin, and lead showed no involvement in this pigmentation in inner tissues of LP–BBS (Additional file 1: Fig. S2A, B).

We compared the characterization of LP–BBS and LP–NBS, and found that they exhibited similar fur color and body size (Additional file 1: Fig. S3A). However, LP-BBS displayed distinct hyperpigmentation in both external (eyelid, gingiva, anus, vulva, abdominal skin) and internal tissues (heart, kidney, liver, spleen, lung, trachea, bronchiole, intestinal tract, dorsal muscle, urinary bladder, ovary, and uterus) (Fig. 1A, Additional file 1: Fig. S3B–D). Their blood appeared dark black (Additional file 1: Fig. S3E). Internal tissues such as kidney showed varying degrees of hyperpigmentation among different individuals (Additional file 1: Fig. S3F).

Histological analysis revealed pigment distributed within almost all the internal tissues, including circulation system, immune system, reproductive system, respiratory system, movement system, and digestive system (Fig. 1B, Additional file 1: Fig. S4). The pigment particles showed closely relationship with circulation when it was prominently in hepatic sinusoid, lymph sinus, splenic sinuses and endothelial cells of blood vessels, and significantly accumulated in reticuloendothelial cells, macrophages, hepatocytes, bronchial chondrocytes, renal capsule endothelial cells, renal tubular epithelial cells, and collecting tubular epithelial cells (Fig. 1B, Additional file 1: Fig. S4). Ultrastructural analysis showed the pigment was different from the melanin in Silky Fowl with obvious melanosomes, which were irregularly shaped and membrane-bound in renal tubular epithelial cells of LP-BBS (Fig. 1C). Given its specific distribution, it was speculated that the pigment might be associated with hemoglobin metabolism, as LP–BBS had higher red blood cell counts and hemoglobin concentration (Fig. 1D, Additional file 2: Table S1), and significant iron overload and reduced transferrin were in their blood and pigmented kidney tissues (Fig. 1E, F, Additional file 2: Table S1).

We further extracted and identified the pigment from LP–BBS kidney, liver, spleen, and muscle, using melanin from Silky Fowl and hemoglobin-derived pigments as control. The extracted pigment showed dark as melanin from Silky Fowl, but only dissolved similarly to the standard pigment hemin (Additional file 1: Fig. S5A). High–performance liquid chromatography (HPLC) compared the extracted pigment to melanin from Silky Fowl and standard hemoglobin-derived pigments (protoporphyrin IX, bilirubin, biliverdin, and hemin), revealing a similar absorption peak to heme metabolic pigment at nearly 13 min (Fig. 1G, Additional file 1: Fig. S1F, 5B). HPLC-mass spectrometry (HPLC-MS) further confirmed the pigment's similarity to ferriheme (hemin without $CL^-$) at 8–8.5 min (Fig. 1H).

According to the ferriheme distribution, we analyzed its effects in LP–BBS organs. The qPCR showed *GPX1* and *SEPW* were highly expressed in spleen and kidney (Fig. 2A). Elevated glutathione peroxidase (*GSH-PX*) and malondialdehyde (*MDA*) levels were found in LP–BBS serum (Fig. 2B, Additional file 3: Table S2). These results revealed ferriheme overload induced severe oxidative stress in the tissues of LP–BBS. In addition, ferriheme overload in the kidney caused severe renal tubular epithelial cell damage, including brush border shedding and organelle degradation, leading to cell death (Fig. 2C). Ferriheme overload induced cell injury resulting in systemic inflammation when immune cells infiltration was significantly noted in the kidney, liver, lung, and lymph node, including lymphocytes, neutrophils, eosinophils, and macrophages (Fig. 2D). Notably, ferriheme overload in reproductive system, the ovarian germinal epithelium and uterine lamina propria, resulted in follicular atresia and cell necrosis (Fig. 2E).

#### Aberrant hemoglobin metabolism and transport pathways in LP–BBS

To explore the mechanism behind ferriheme overload in LP–BBS, transcriptomic data from spleen, liver, and kidney tissues with significant ferriheme overload were analyzed (Additional file 3: Tables S3). Differentially expressed genes (DEGs) were identified in spleen (637 with 328 upregulated and 309 downregulated), kidney (804 with 404 upregulated and 400 downregulated), and liver (1,100 with 551 upregulated and 549 downregulated) (Fig. 3A, Additional file 2: Tables S4–6). The differentially expressed genes linked to NADPH dehydrogenase activity, redox function, and oxygen transport, including *FOS*, *JUN*, *GPX1*, *SELENOW*, *EFHB*, and *RNMT*, were co-regulated in the spleen, kidney, and liver (Fig. 3B–D, Additional file 3: Table S7). These results further revealed ferriheme overload induced severe oxidative stress in the tissues of LP–BBS.

In addition, DEGs associated with heme binding, hemoglobin complex, oxygen binding, oxygen transport, iron ion binding, and blood microparticles were enriched in the spleen (Fig. 3D). The 5'-aminolevulinate synthase 2 (*ALAS2*) gene, crucial enzyme for heme biosynthetic, was differentially detected in spleen of LP–BBS (Fig. 3E, Additional file 2: Table S4, Additional file 3: Table S8, 9).

In the kidney, genes related to blood microparticle, transmembrane transport, ion transport, metabolic process, and transport activity, such as *SLC4A1* and *TFRC*,

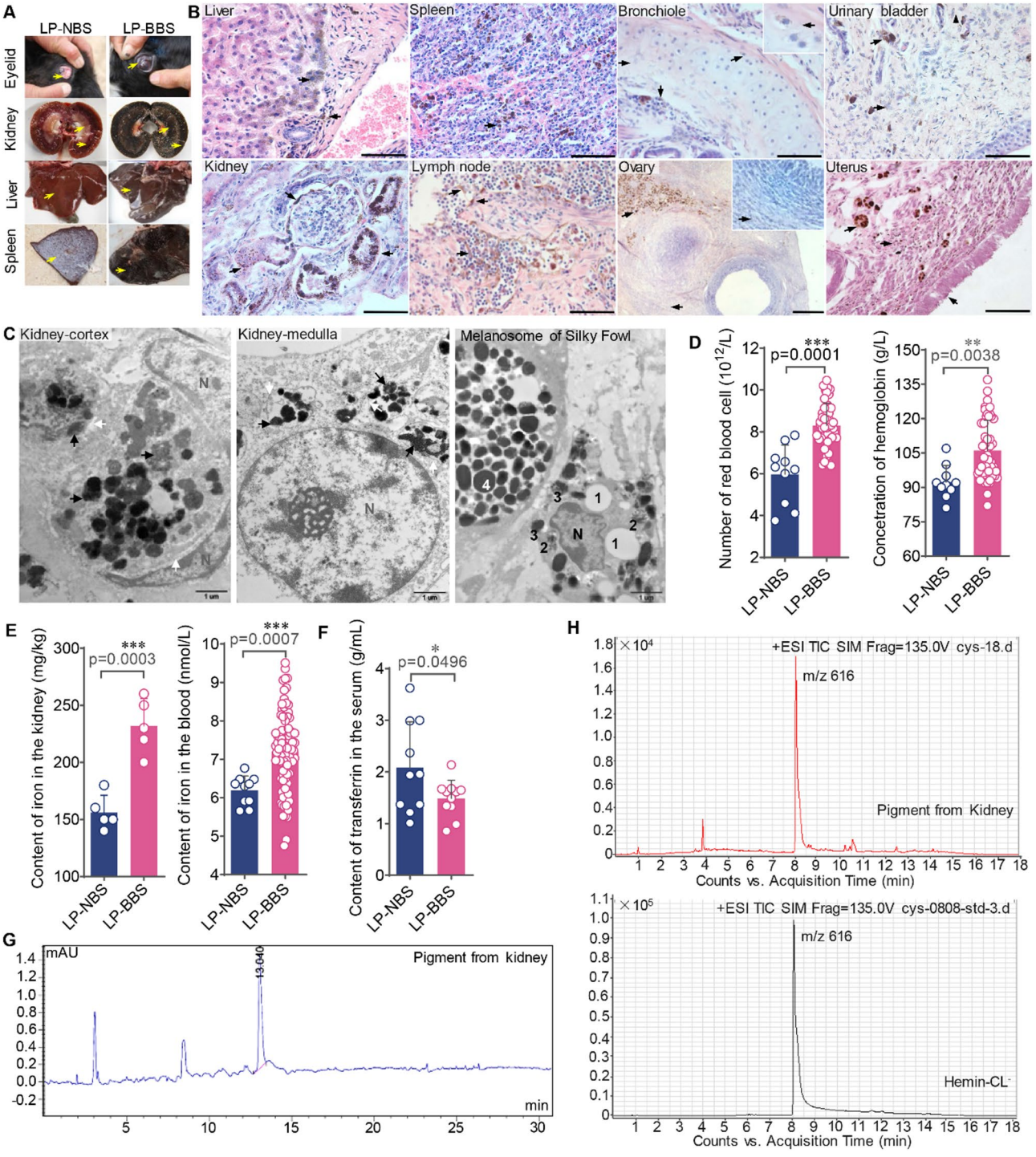


**Fig. 1** LP–BBS hyperpigmentation characterization. **A** Hyperpigmentation phenotype of inner tissues from LP–BBS. **B** Histological distribution of pigment in the inner tissues. Bar = 100 μm. **C** Ultrastructure of pigment (black arrow) capsuled with membrane (white arrow) in the renal tubular epithelial cells and collecting tubular epithelial cells. Different stages of melanosomes were observed in the melanocytes of Silky Fowl. N, nucleus. 1–4, one to four stages of melanosome. **D** More number of red blood cells and concentration of hemoglobin in blood. Data are mean ± SEM. Unpaired two-sided Student's *t*-test ($^{*}p < 0.05$, $^{**}p < 0.01$, $^{***}p < 0.001$). **E** Iron contents in the kidney and blood. **F** Level of transferrin in the blood. **G** Absorption peak value of pigment from LP–BBS by HPLC analysis. **H** Pigment showed similar peak value to the hemin

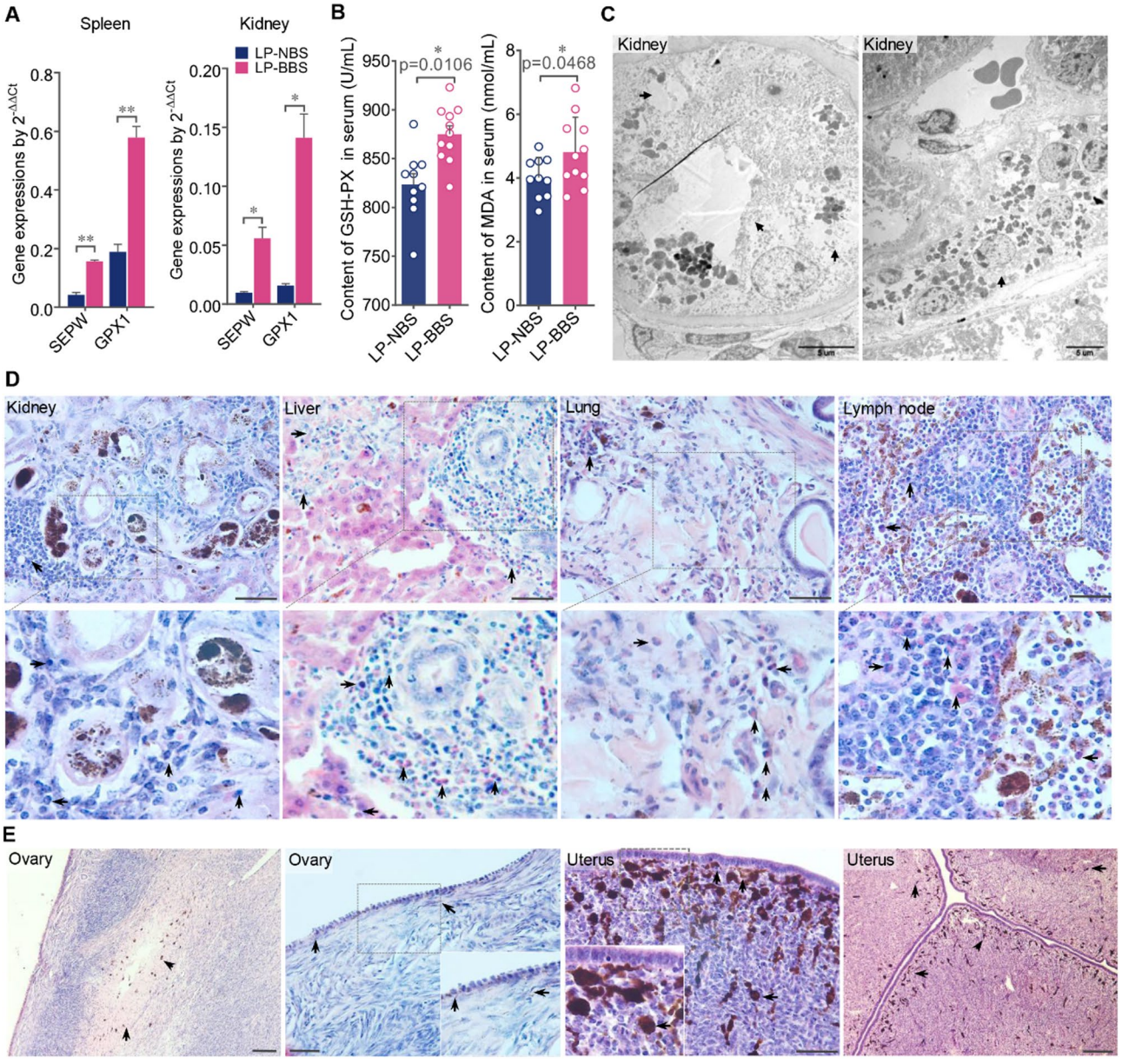


**Fig. 2** Pathological analysis of LP–BBS. **A** Higher expressions of *SEPW1* and *GPX1* are significantly detected in the spleen and kidney of LP–BBS ($n = 3–5$) by qPCR. LP–NBS ($n = 3–4$) from same indigenous population; Data are mean ± SEM. Unpaired two-sided Student's *t*-test ($^{*}p < 0.05$, $^{**}p < 0.01$). **B** Higher levels of GSH-PX ($p = 0.0106$) and more contents of MDA ($p = 0.0468$) are detected in the blood of LP–BBS ($n = 11$). LP–NBS ($n = 10$) from same indigenous population; Data are mean ± SEM. Unpaired two-sided Student's *t*-test. **C** Severe bursting of cell membranes and organelles shown as swollen, vacuolated and broken are in the renal tubular epithelial cells. **D** Obvious inflammatory cells infiltrated in the kidney, liver, lung and lymph node (arrow). **E** Follicular atresia and cell necrosis were in the ovary and uterus when ferriheme overload notably in the germinal epithelium and atretic follicle of the ovary, and in the lamina propria of uterus. Bar = 100 μm

were significantly downregulated (Additional file 1: Fig. S6A, Additional file 2: Table S5). In the liver, upregulated genes were enriched in intracellular membrane–bound organelles, transport vesicle membranes, and melanin biosynthetic process regulation (Additional file 1: Fig. S6B; Additional file 2: Table S6). In which, genes encoding *ABCB6*, *SFXN1*, *STEAP3*, and *TRFC*, crucial for cellular iron ion homeostasis, were differentially expressed in the LP–BBS liver (Additional file 2: Table S6).

Notably, genes related to hemoglobin synthesis and metabolism were differentially detected in the spleen, kidney, and liver between LP–BBS and LP–NBS (Fig. 3F). Specifically, genes associated with heme metabolism were significantly enriched in the spleen of LP–BBS (Fig. 3G).

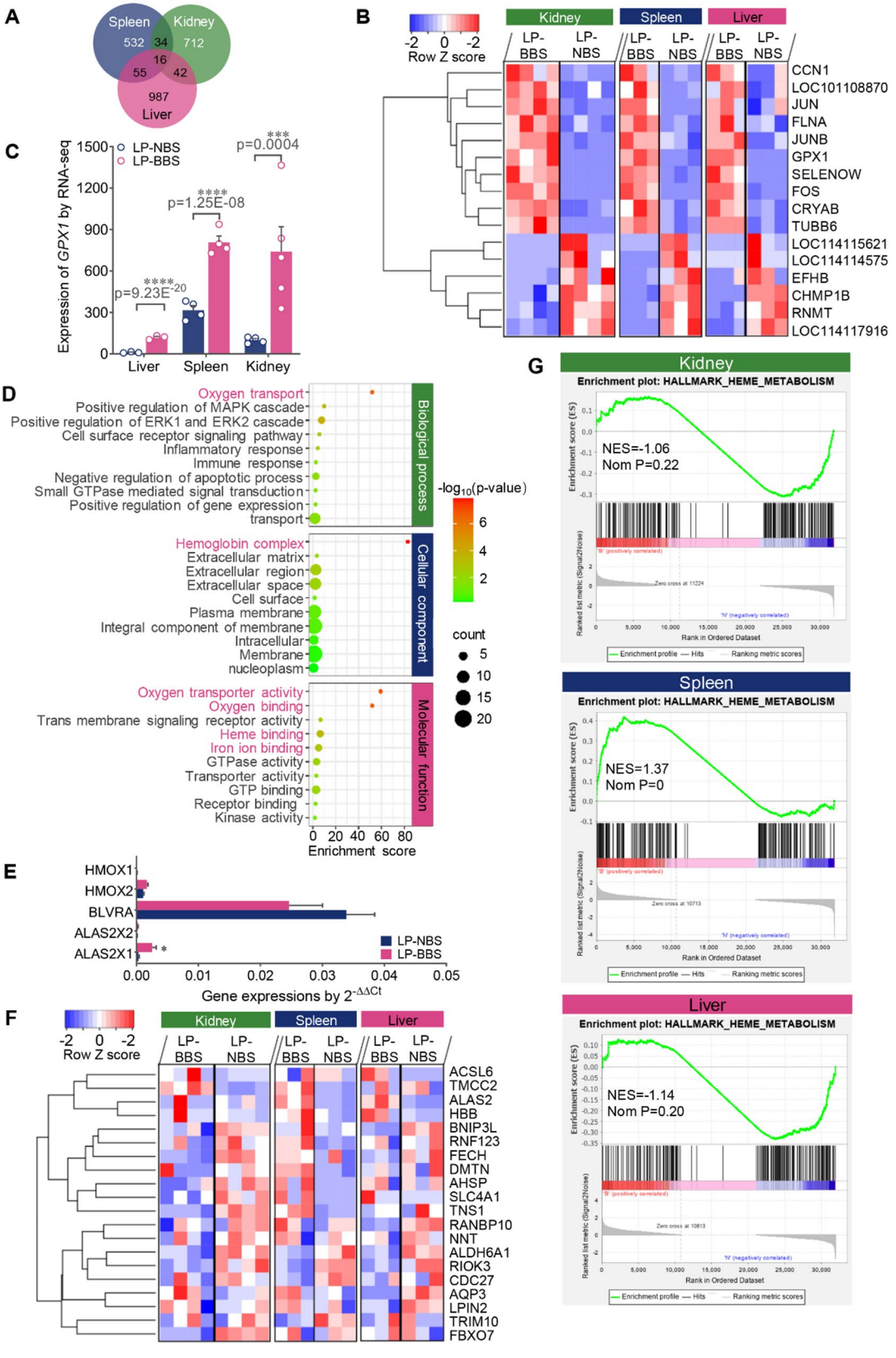


**Fig. 3** (See legend on next page.)

(See figure on previous page.)

**Fig. 3** Ferriheme overload characterization in LP–BBS. **A** Numbers of DEGs identified in the spleen, kidney and liver. **B** Co-regulated genes in the spleen, kidney, and liver of LP–BBS. **C** Higher expressions of *GPX1* were significantly detected in the liver, spleen and kidney of LP–BBS ($n = 3–5$). LP–NBS ($n = 3–4$) from same indigenous population; Data are mean ± SEM. Unpaired two-sided Student's *t*-test. **D** Enriched GO terms from DEGs in the spleen. **E** Higher expressions of *ALAS2* was detected in the spleen of LP–BBS by qRT-PCR; Data are mean ± SEM. Unpaired two-sided Student's *t*-test ($^{*}p < 0.05$, $^{**}p < 0.01$). **F** Heatmap of DEGs related to hemoglobin synthesis and metabolism. **G** Genes related to heme metabolism were enriched in the spleen, liver, and kidney of LP–BBS by GSEA

### Genome sequencing and genome wide association study identified key variation in *FRRS1L*

LP–BBS is the only natural population of black-bone sheep found in the Hengduan Mountains (HDMs) with different altitudes in Yunnan province (Fig. 4A). To elucidate genetic mechanism of ferriheme overload in LP–BBS, we collected different sheep populations for next generation sequencing (NGS) and analyzed their genomic selection signals. It includes LP–BBS ($n = 16$), and LP–NBS ($n = 5$) from HDMs, and five other non-black bone sheep (NBS) populations from Yunnan and Tibetan regions ($n = 26$) (Fig. 4A, Additional file 3: Table S10, 11). Based on the top 5% of Fst values (Z(Fst) > 2.05) and θπ ratio cutoffs ($\log_2\theta\pi$(BBS/NBS) > 0.37), we screened 677 outlier genes in LP-BBS (Fig. 4B, Additional file 2: Table S12). According to their annotated functions, all outlier genes could be clustered into 33 Gene Ontology (GO) terms (Fig. 4C), where those associated with development, postsynaptic membrane, synapse, cholinergic synapse, and dopamine metabolic process were highly enriched, indicating their contribution to the differential adaptive response of LP-BBS. Significantly expressed genes related to ion channels, ion transport, metal binding, magnesium, zinc, and transferase-possibly linked to heme metabolism and iron transport were also identified in LP-BBS (Fig. 4C).

To further uncover the key genes causing ferriheme overload, selective breeding efforts since 2001 has been performed and we established a population with distinct ferriheme overload trait. Our crossbreeding experiments with male LP-BBS ($n = 3$) and female Suffolk sheep ($n = 42$) demonstrated that ferriheme overload was a major gene or polygenic controlled trait, as both black bone and non-black bone phenotypes were observed in male and female hybrids, and the degree of pigmentation in black bone sheep is not the same (Additional file 1: Fig. S7). Genome-wide association studies (GWAS) using these crossbreeding population ($n = 42$) was applied in the xpEHH analysis to sweep genomic differentiation sites, the identified candidate SNPs with significant loci mapped on chromosome 2 and other chromosomes (Fig. 4D). When overlap the GWAS result with the NGS selection signals, ferric chelate reductase 1 like (*FRRS1L*) gene on chromosome 2 was located in the intersection (Fig. 4E, Additional file 2: Table S13), which contains a transmembrane and extracellular dopamine beta-monooxygenase N-terminal (DOMON) domain associated with heme and sugar recognition. The changes in *FRRS1L* function may cause ferriheme overload in different internal tissues. There are two single nucleotide polymorphisms (SNPs) in the 3'-untranslated region (3'-UTR) of *FRRS1L* that provide significant signals, namely the 4852 bp G > T mutation and the 1016 bp C > A mutation. In a natural population of LP-BBS ($n = 64$) and LP-NBS ($n = 44$), it was found that they both exhibited specificity in LP–BBS: their frequencies were T = 0.92 (reference allele G = 0.08) and A = 0.79 (reference allele C = 0.21), respectively, while in the LP–NBS populations, the allele frequencies of these two mutations were zero (T = 0 and A = 0, reference allele G = 1, C = 1; Fig. 4F). The genotypic data indicates that the LP–NBS are homozygous for both SNPs (TT and AA), while the LP–BBS are either homozygous (GG and CC) or heterogeneous (TG and AC). Therefore, the inherence of hyperpigmentation is likely a dominant trait modified by multiple genes. These results suggest that *FRRS1L* can serve as a candidate gene for hyperpigmentation analysis.

### 3′-UTR mutation in *FRRS1L* results in its lower expression contributing to Ferriheme overload

In order to screen for other variations in *FRRS1L* gene, Sanger sequencing was performed on the full sequence of this gene using mixed pool DNA from LP–BBS ($n = 20$) and LP–NBS sheep ($n = 5$). Six SNPs (SNP1–6) were identified in the 3′-UTR region of *FRRS1L* (Fig. 5A, Additional file 3: Table S14). Of these, the two SNPs identified through our NGS analysis were included named SNP2 (1,016, A/C) and SNP6 (4,852 bp, T/G). In order to further analyze the impact of the six SNPs on *FRRS1L* expression, luciferase reporter gene expression assay was performed for each SNP. The result showed that SNP2 and SNP6 significantly reduced the expressions of luciferase especially the SNP6 ($p = 0.0021$, Fig. 5B, Additional file 3: Table S15), which suggested the key variation reduced *FRRS1L* expression in LP–NBS. This conclusion was consistent with the results of quantitative RT-PCR and immunohistochemistry for FRRS1L, which revealed significantly lower expressions of *FRRS1L* in LP–BBS tissues than that in LP–NBS tissues (Fig. 5C–E, Additional file 1: Fig. S8A, Additional file 3: Table S16, 17).

The macrophages with ferriheme overload were evidently observed in inner tissues in vivo (Fig. 6A), so to link *FRRS1L* downregulation with ferriheme overload, we used primary alveolar macrophages from Hu sheep

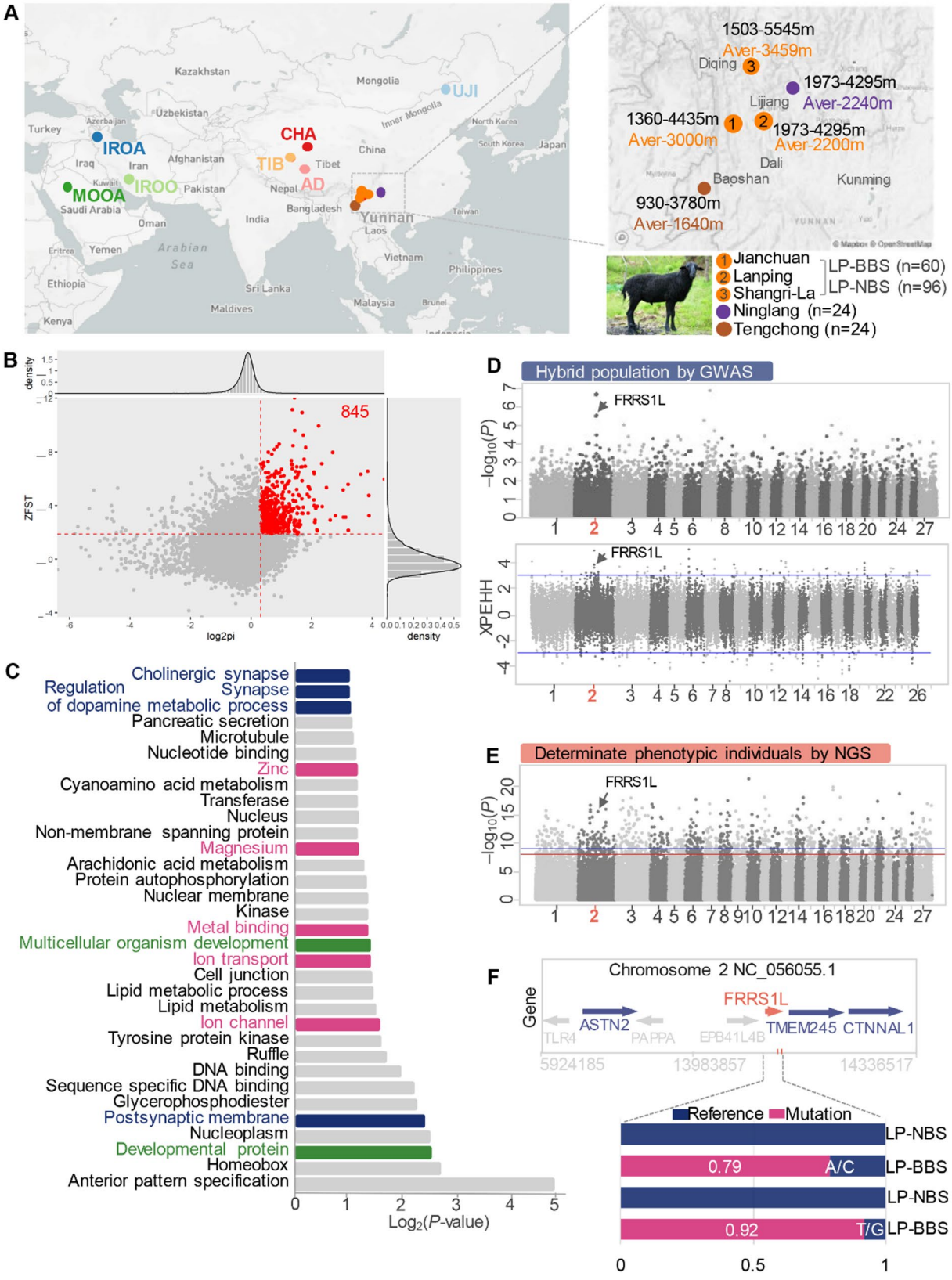


**Fig. 4** (See legend on next page.)

(See figure on previous page.)

**Fig. 4** The selection signals of LP–BBS genomes and *FRRS1L* locus. **A** Geographical distribution and sampling of LP–BBS in Lanping, Jianchuan, and Shangri-La, Yunnan province, along the HDMs with different high altitudes. The map is from Google Maps (map data © 2016 Google, SK Planet, ZENRIN). **B** Distribution of $\log_2$ (hp ratios) and Z ($F_{ST}$) values calculated in 100-kb sliding windows with 50-kb increments between LP–BBS and LP–NBS, and 845 genes were identified. **C** Enriched terms of the screened genes by NGS. **D** Manhattan plots from determinate phenotypic individuals of hybrid population showed the significance and location distribution of SNPs with threshold as–$\log_{10}$ ($5e^{-8}$) and–$\log_{10}$ ($5e^{-9}$). **E** Manhattan plot of the results from the determinate phenotypic individuals by NGS. **F** The located genes *FRRS1L* with two SNPs, *ASTN2*, *TMEM245*, and *CTNNAL1* in Chromosome 2. Population genetic analysis revealed gene variation frequencies of the two mutated sites in the *FRRS1L* 3′-UTR. One is a T/G mutation at the 4,852 bp from the end of the 3′-UTR (frequencies of gene variation is 0.92), and the other is an A/C mutation at the 1,016 bp from the end of the 3′-UTR (frequencies of gene variation is 0.79). HDMs, Hengduan Mountains; NGS, next generation sequencing

(a Chinese local breed with no hyperpigmentation) to elucidate. When exposing them to LP–BBS ferriheme, macrophages internalized the ferriheme (Fig. 6B) i*n vitro* accompanied by marked upregulation of genes linked to immune responses, apoptosis, and 3'-UTR-mediated mRNA destabilization, whereas a concurrent downregulation of metabolic related genes is observed (Additional file 2: Table S18–23), indicating ferriheme overload in vivo partially related to cytophagocytosis. Furthermore, *ALAS1* and *FECH* as key genes for heme synthesis were detected in macrophages (Fig. 6C) illustrating itself could synthesize protoporphyrin or heme, and downregulating *FRRS1L* or *FRRS1* via RNA interference caused pigment accumulation in cytoplasm (Fig. 6D, Additional file 3: Table S24). HPLC analysis confirmed the pigment accumulated in macrophages was ferriheme (Fig. 6E, F). Additionally, it was noted expressions of *ALAS1* and *FECH* significantly increased following ferriheme accumulation (Fig. 6C, Additional file 3: Table S25).

## Discussion

While previous studies on hyperpigmentation in Lanping black bone sheep (LP–BBS) have focused on melanogenesis pathways due to the unclear chemical nature of the black substances [13, 23–27], our findings reveal that the condition arises from a disorder a hemoglobin metabolism. Specifically, impaired ferric iron reduction in macrophages and reticuloendothelial cells leads to systemic ferriheme accumulation (Additional file 1: Fig. S9). This mechanism mirrors iron-related disorders in humans, such as hemochromatosis, methemoglobinemia, and aceruloplasminemia [28–34], with LP–BBS also exhibiting analogous pathological features.

Our data suggest that hyperpigmentation in LP–BBS does not follow a simple Mendelian inheritance pattern. Instead, the phenotype appears to be polygenic and potentially influenced by gene-environment interactions. Unlike previous reports, they found that hyperpigmentation can be linked to mutations in genes like *HFE*, *HJV*, *HAMP*, *TFR2*, *SLC40A1* (*ferroportin 1*), and *CYB5R* [29–35], our study did not detect significant variations in these genes in LP–BBS. Instead, we identified *FRRS1L* as a key gene implicated in iron overload in LP–BBS. This gene has not been previously reported in human heme metabolism disorders. Research on *FRRS1L* deficiency has primarily linked it to neurodevelopmental and motor abnormalities due to its role as a component of AMPA receptor complexes [36–38].

*FRRS1L* is highly expressed not only in the central nervous system (CNS) but also in the kidney, liver, and testis [39, 40]. Our findings showed that in sheep, *FRRS1L* is prominently expressed in the kidney, lung, lymph node and spleen, particularly in reticuloendothelial cells and alveolar macrophages. Unlike its role in neurons, *FRRS1L* in macrophages is crucial for ferric iron reduction, possibly due to its transmembrane and extracellular DOMON domain associated with heme and sugar recognition [41]. In addition, on chromosome 2, lncRNAs and microRNAs were also annotated in LP–BBS, and microRNAs predicted to target the identified key variation in the 3′-UTR of *FRRS1L* were identified (Additional file 2: Table S26). These may be strongly associated with lower FFRS1L expression in internal tissues, and could contribute to modulate gene expressions epigenetically, resulting in varying degrees of ferriheme overload in LP–BBS. In addition, our in vitro experiment revealed that intracellular accumulation of ferriheme in macrophages did not induce ferroptosis, but rather triggered immune response activation (Additional file 2: Table S18–23). Concurrently, we observed significant upregulation of genes associated with apoptotic process and 3'-UTR-mediated mRNA destabilization in macrophages (Additional file 2: Table S18–23). These findings suggest that ferriheme accumulation does not significantly induce ferroptosis, likely due to the iron remaining in a non-labile state. In this state, iron is tightly bound within a molecule or complex and is not readily available for chemical reactions or exchange with other molecules.

Furthermore, in our in vivo experiment, we identified macrophages and reticuloendothelial cells as the primary cell types accumulating ferriheme. Given their inherent capacity for phagocytosis and clearance of foreign substances, we subsequently focused on characterizing the physiological consequences of ferriheme accumulation in macrophages. However, the impact of ferriheme accumulation in other cell types remains to be elucidated.

In addition to *FRRS1L*, genes such as *HIF1A*, *MOXD1*, and *KCNH2*, which are involved in hypoxia adaptation, showed higher expression in LP–BBS spleen and liver (Additional file 1: Fig. S10, Additional file 3: Table

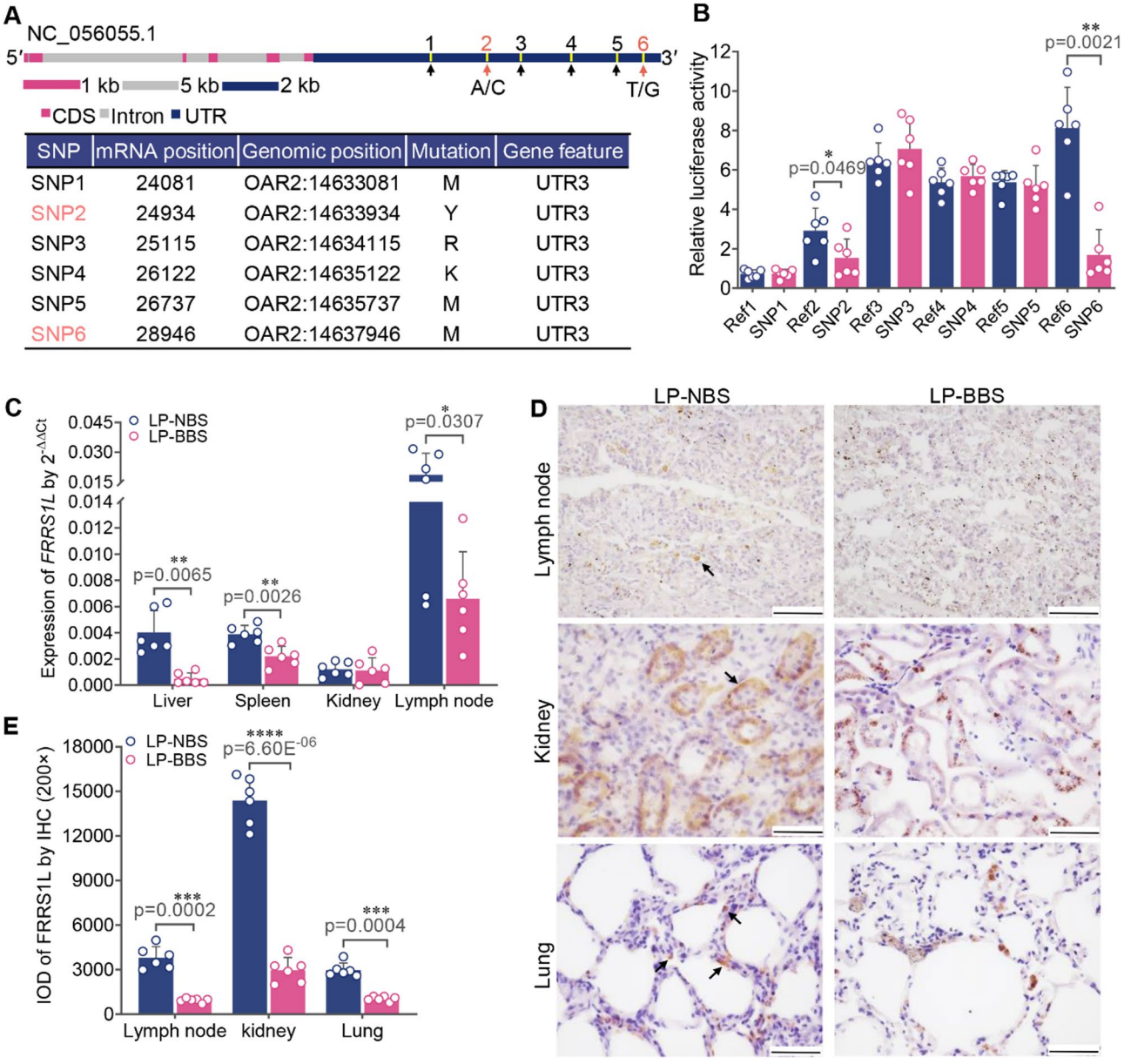


| SNP | mRNA position | Genomic position | Mutation | Gene feature |
|---|---|---|---|---|
| SNP1 | 24081 | OAR2:14633081 | M | UTR3 |
| SNP2 | 24934 | OAR2:14633934 | Y | UTR3 |
| SNP3 | 25115 | OAR2:14634115 | R | UTR3 |
| SNP4 | 26122 | OAR2:14635122 | K | UTR3 |
| SNP5 | 26737 | OAR2:14635737 | M | UTR3 |
| SNP6 | 28946 | OAR2:14637946 | M | UTR3 |

**Fig. 5** The key variation of *FRRS1L* in LP–BBS genomes. **A** Six mutation sites in the *FRRS1L* 3′-UTR by mix pool sequencing in LP–BBS ($n=20$) and LP–NBS ($n=5$). **B** SNPs at the 1,016 bp and 4,852 bp from the end of 3′-UTR downregulated the reporter gene's expression. $n=6$ per group; Data are mean ± SEM. Paired two-sided Student's *t*-test ($^{*}p<0.05$, $^{**}p<0.01$). **C** Expressions of *FRRS1L* in the inner tissues by qRT-PCR. Data are mean ± SEM. Paired two–sided Student's *t*-test ($^{*}p<0.05$, $^{**}p<0.01$). **D** FRRS1L is markedly expressed in the lymph node (reticuloendothelial cell), kidney (renal tubular epithelial cell), and lung (macrophage and alveolar epithelial cell). **E** Significant lower expression of FRRS1L in LP–BBS ($n=6$). Data are mean ± SEM. Paired two-sided Student's *t*-test ($^{***}p<0.001$, $^{****}p<0.0001$). IOD, integral optical density

S27). The PAS domain in *HIF1A* and *KCNH2* and the DOMON domain in *MOXD1* facilitate responses to various environmental factors, such as diatomic gases, light, and redox potential, which are known to require the cofactors heme, flavin mononucleotide (FMN), parahydroxycinnamate, and flavin adenine dinucleotide (FAD) [42]. The DOMON domain, initially thought to enable protein-protein interactions, was subsequently identified as a heme binding motif in cellobiose dehydrogenase [41]. The significantly increased expression levels of *HIF1A* and *MOXD1* in LP–BBS likely enhances hypoxic response and accommodation. The Hengduan Mountains (HDMs), located at the intersection of East Asia, South Asia, and the Qinghai Tibet Plateau at altitudes of 1,000–4,500 m, are among the most vulnerable areas among all global biodiversity hotspots due to climate change and anthropogenic disturbances [15, 43]. Past geological and climatic changes in the HDMs may have created

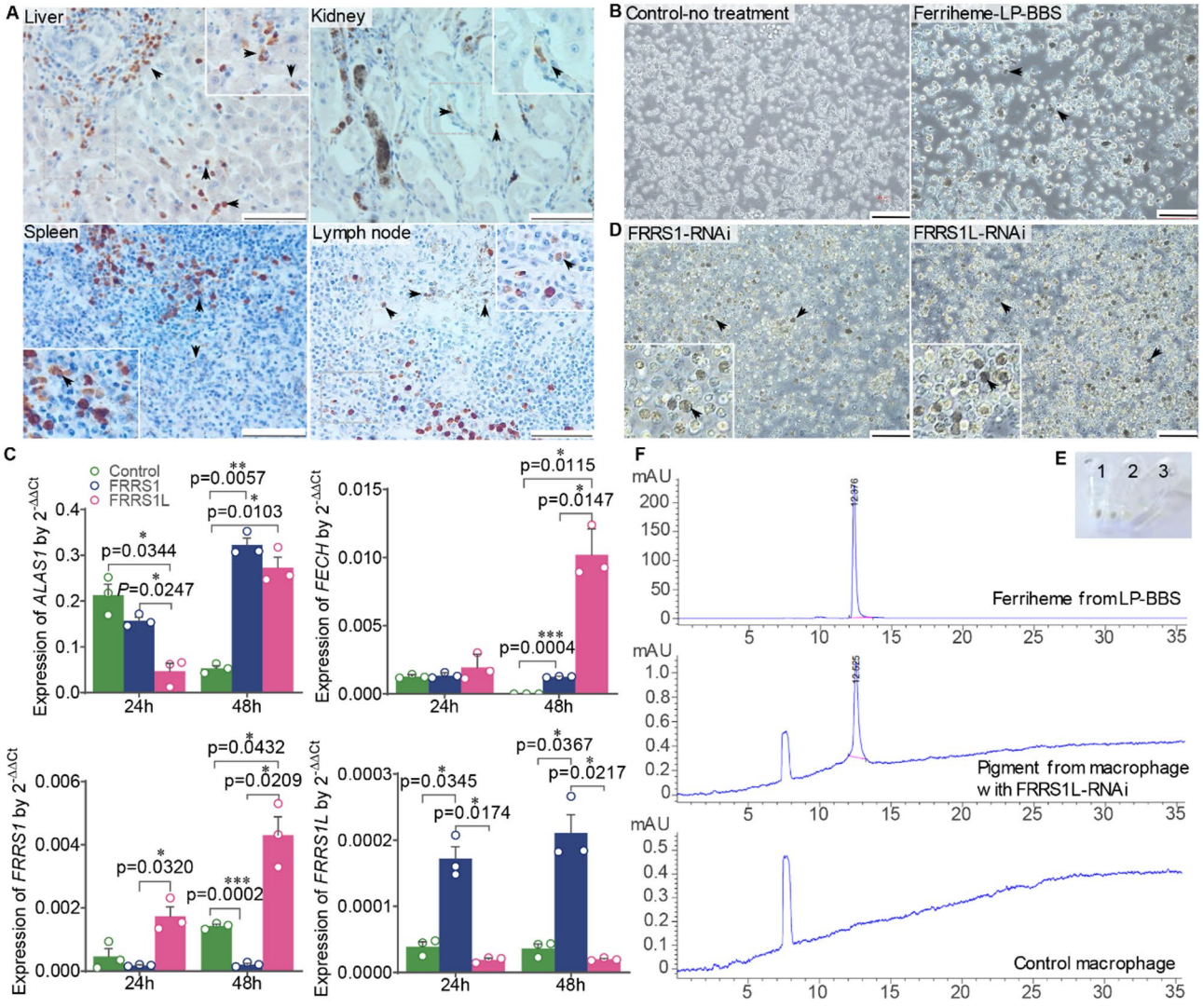


**Fig. 6** The association between FRRS1L and hyperpigmentation. **A** Ferriheme is present in macrophages from different inner tissues. Immunohistochemistry. Bar = 100 μm. **B** Ferriheme extracted from LP–BBS is engulfed by alveolar macrophages at 24 h in vitro. Control: no ferriheme treatment; Bar = 20 μm. **C** Macrophages express *ALAS1*, *FECH*, *FRRS1*, and *FRRS1L*, which are involved in heme synthesis and metabolism. Downregulated expression of *FRRS1* and *FRRS1L*, *ALAS1* and *FECH* significantly increases at 48 h. $n = 3$ per group; Data are mean ± SEM. Paired two-sided Student's *t*-test ($^{*}p < 0.05$, $^{**}p < 0.01$, $^{***}p < 0.001$). **D** Downregulating *FRRS1* and *FRRS1L* expressions in macrophages via RNA interference induces pigmentation in the cytoplasm of macrophage (arrow). Bar = 20 μm. **E** Pigment accumulated in the macrophages was extracted via cell lysis (1, *FRRS1*–RNAi. 2, *FRRS1L*–RNAi. 3, Control–Negative RNAi). **F** Pigment in the macrophage was identified as being the same as ferriheme in LP–BBS using high–performance liquid chromatography

microhabitat differentiation, promoting local adaptation, ecological divergence, and lineage diversification [15].

LP–BBS have only been discovered in Lanping, Jianchuan, and Shangri-La, Yunnan province, all of which are located along HDMs at high altitudes ranging from 2,000 to 4,000 m. High altitudes greatly contribute to the adaptation and evolution of animals and humans [44–49]. The hyperpigmentation phenotype of LP–BBS becomes more obvious with increasing altitude; however, this phenotype weakens after more than two generations in low-altitude areas, including Beijing, Shandong Province, and the Inner Mongolia Autonomous Region in China. Therefore, the high altitudes and hypoxic environments along the HDMs may lead to accelerated gene variation and modulation of biological pathways in LP–BBS for adaptation purposes. The hypoxia atmosphere and microenvironment increase vascular permeability, prompting ferriheme infiltration into internal tissues during blood circulation.

Although *FRRS1L* has been predominantly studied in the context of AMPA receptor regulation and neurodevelopmental disorders in humans [36–38], our findings suggest that this gene may also play a previously unrecognized role in systemic iron homeostasis, particularly in macrophage-mediated ferric iron reduction. This is supported by its strong expression in the kidney, lung,

lymph nodes, and spleen of LP–BBS—tissues enriched in reticuloendothelial cells—as well as the presence of a transmembrane DOMON domain, which is implicated in heme and redox-related molecular interactions [41]. *FRRS1L*'s functional divergence may be species-specific or context-dependent, potentially driven by differences in tissue-specific expression or post-transcriptional regulation, such as the 3′-UTR mutation we identified that may alter microRNA-mediated repression.

Notably, *FRRS1L* is expressed in both the central nervous system (CNS) and peripheral tissues (e.g. liver and kidney) in sheep and humans [39, 40], implying uncharacterized broader roles. While no direct evidence currently links *FRRS1L* to iron overload disorders in humans, our findings offer a natural model to investigate noncanonical pathways of ferriheme clearance and iron homeostasis. These results should be considered hypothesis-generating. Future studies including functional assays and population-based genetic analyses in humans and other species, will be necessary to determine whether *FRRS1L* variants or dysregulation contribute to iron-related pathologies [50], especially under hypoxic stress.

## Conclusion

This study presents a natural mammalian model of ferriheme overload in LP–BBS sheep, where hyperpigmentation results from aberrant hemoglobin metabolism rather than melanogenesis. We identify *FRRS1L* as a candidate gene, potentially downregulated via a 3′-UTR mutation affecting ferric iron reduction in macrophages. Environmental stressors, particularly high altitude hypoxia, may accelerate ferriheme accumulation through gene–environment interactions. While *FRRS1L* has not been linked to iron metabolism in humans, our findings suggest a novel, species-specific role. This model offers new insights into iron-related pathologies and highlights the need for functional studies and validation in human and other animal systems.

## Methods

### Animals

The populations of LP–BBS and LP–NBS from indigenous sheep, both male and female, aged 1–3 years, were selected from Lanping County, Jianchuan County, Shangri-La City of Yunnan province. LP–NBS was confirmed by dissection and visual inspection of their eyelid, gingiva, anus, and skin of abdomen. The other control sheep populations, also male and female aged 1–3 years were from Ninglang County and Tengchong County, Tibet, and Inner Mongolia Autonomous Region. Previously published SNP data and sequencing data were downloaded and included in this study to analyze genetic variations. Blood samples were collected from jugular vein, and the corresponding tissues of selected LP–BBS and LP–NBS individuals were sampled.

### Histological analysis

LP–NBS ($n = 10$: four from Jianchuan, three from Lanping, and three from Shangri-La) and LP–BBS ($n = 11$ from Jianchuan, $n = 49$ from Lanping, $n = 92$ from Shangri-La) were selected. Visible inspection of overall appearance, coat, eyelid, gingiva, and anus colors was performed. Blood was collected from the jugular vein, and analyzed for the red blood cells, hemoglobin, iron, lead, zinc, copper, selenium (Beijing Huaying Institute of Biotechnology, Beijing, China). The heart, liver, spleen, lung, kidney, trachea, intestines, lymph node, ovary, uterus, uterine tube, bladder, skin, longissimus dorsi, pulmonary artery were sampled from 16 LP–BBS (eight from Lanping County and eight from Shangri-La City) and five LP–NBS (Lanping County), aged 2–3 years. Samples were fixed in 4% paraformaldehyde solution, processed for paraffin sections. After staining with H&E, sections were histologically examined. The Ultrathin sections of hyperpigmented kidney of LP–BBS and skin of Silky Fowl were examined for melanosomes under a transmission electron microscope (JEM-1230, Japan).

### Pigment confirmation

The tissues ($n = 5$ for LP–BBS, $n = 5$ for LP–NBS) were prepared as serial frozen sections to determine melanin. Anti-S100 monoclonal antibody (1:200, ab34686, Abcam Biotechnology Co., Ltd., Shanghai, China), anti-MiTF polyclonal antibody (1:500, ab122982, Abcam Biotechnology Co., Ltd., Shanghai, China), and 3, 4-Dihydroxy-L-phenylalanine (DOPA, Sigma Aldrich, Shanghai, China) staining were used to label melanocytes. Genes for tyrosinase (*TYR*), Melanocortin 1 Receptor (*MC1R*), and Agouti related to melanin synthesis in kidney ($n = 5$–10 for both LP–BBS and LP–NBS groups) were detected by semi-quantitative analysis. Total RNA was extracted from liver, spleen, kidney, and periosteum ($n = 5$ for LP–BBS, $n = 5$ for LP–NBS) using RNAprep Pure Tissue Kit (DP431, TIANGEN Biotech Co., Ltd., Beijing, China). After purification (Qiagen) and quality assessment, the RNA was reverse transcribed with FastQuant RT Kit (with gDNase) (KR118, TIANGEN Biotech Co., Ltd., Beijing, China). Semi-quantitative analysis of *TYR*, *MC1R* and *Agouti* genes relative to *GAPDH* was performed using the TIANGEN Taq Master Mix (KT211, TIANGEN Biotech Co., Ltd., Beijing, China).

Hemosiderin and melanin were examined by improved Prussian blue staining. Paraffin sections ($n = 10$ for LP–BBS, $n = 10$ for LP–NBS) were immersed in 2% potassium ferrocyanide (Sinopharm Chemical Reagent Beijing Co., Ltd., Beijing, China) and 2% hydrochloric acid, 1:1 (v/v; Sinopharm Chemical Reagent Beijing Co., Ltd., Beijing,

China) for 15 min. Sections were rinsed with distilled water and then placed into fresh 1% potassium permanganate, until the sections appeared yellowish-brown. Rinsed with distilled water, the sections were then incubated in 1% oxalic acid (Sinopharm Chemical Reagent Beijing Co., Ltd., Beijing, China) for 10 min. After being rinsed and counterstained with hematoxylin (Solarbio Technology Co., Ltd., Beijing, China), the sections were dehydrated and mounted. Hemosiderin and melanin appeared as blue and colorless, respectively, under the microscope.

Frozen sections ($n = 10$ for both LP–BBS and LP–NBS groups) were rinsed with PBS, incubated in 2% potassium ferricyanide for 5 min, then incubated in 2% potassium ferricyanide (Sinopharm Chemical Reagent Beijing Co., Ltd., Beijing, China) and 5% acetic acid (1:1, Sinopharm Chemical Reagent Beijing Co., Ltd., Beijing, China) for 20 min. After being rinsed with tap water, the sections were incubated in 3% potassium dichromate (Sinopharm Chemical Reagent Beijing Co., Ltd., Beijing, China) for 15 min. Then washed with distilled water, the sections were incubated in 0.5% oil red O-isopropyl alcohol (Solarbio Technology Co., Ltd., Beijing, China) for 10 min. After incubated in 60% ethyl alcohol for 30 s, the sections were washed with distilled water and mounted with glycerinum (Solarbio Technology Co., Ltd., Beijing, China). Under the microscope, the bilirubin and lipofuscin appeared as bright green and dark salmon respectively.

The lead in the kidney ($n = 5$ for both LP–BBS and LP–NBS groups) was stained with the Mallory-Parker method with minor modifications. Frozen sections of the kidney were rinsed with PBS and incubated in 0.1% methylthionine chloride for 15 min. Sections were rinsed with distilled water, transferred to 95% alcohol until the lead appeared dark blue under the microscope, then dehydrated and mounted.

The standard melanin from cuttlefish (Sigma Aldrich, Shanghai, China), melanin from Silky Fowl (extracted and preserved in our laboratory), pigment from kidney, spleen, muscle of LP–BBS were comparatively analyzed for their absorption peaks by high-performance liquid chromatography (HPLC).

#### The iron in the blood and kidney

The frozen kidneys of LP–BBS ($n = 5$) and LP–NBS ($n = 5$) were weighed and freeze-dried using a vacuum freeze-dryer (Shanghai Binlon Instrument Co., Ltd., Shanghai, China), then ground into powder. The iron content in kidney powders and plasma samples ($n = 92$ for LP–BBS, $n = 10$ for LP–NBS) was determined using flame-atomic absorption spectrophotometry.

#### Pigment extraction and structure analysis

All the samples of kidney and spleen from LP–BBS ($n = 5$) were transferred into 50 mL Corning centrifuge tubes. After addition of 20 mL of 0.01 M PBS and 0.25% papain, the tubes were vortex-mixed for 1 min and incubated at 63 °C for 3 h. Then, 0.15% compound protease was added for 2 h at 54 °C. After boiling for 0.5 h to inactivate protease, the homogenate was cooled and filtered through a cell strainer. The suspension was centrifuged at 12,000 r/min for 10 min to collect the crude pigment. The pigment was suspended sequentially with diethyl ether, ethyl alcohol and deionized water respectively, the tubes were vortex–mixed for 1.5 min and were centrifuged at 15,000 r/min for 2 min in a thermo centrifuge and the supernatants were discarded. The pigment was then suspended with tris-saturated phenol, and centrifuged at 15,000 r/min for 1 min. Supernatants were transferred to fresh tubes and kept in the dark at 4 °C until used for HPLC and HPLC/ESI–MS, generally within 24 h of preparation.

Reversed-phase HPLC was conducted with a flow rate of 1.00 mL/min. Solvent A was 0.05% TFA in water and solvent B was acetonitrile. The initial composition was 90% A, 10% B with a linear gradient to 0% A and 100% B at 25 min; the final solvent (acetonitrile) was run isocratically for a further 10 min. Equilibration time was 10 min. Peak detection was at 377 nm up to 15 min and at 405 nm until the end of the run. Biliverdin eluted at 13.7 min, zinc protoporphyrin at 24.5 min and protoporphyrin at 26.0 min. Since the zinc biliverdin complex was unstable at the pH 2.6 of this solvent system, reverting to biliverdin, HPLC of these compounds was done at pH 7.2 with a 0.5 M ammonium acetate (solvent A) and acetonitrile (solvent B) system. The initial composition was 80% A, 20% B, with a linear gradient to 45% A, 55% B at 20 min. Peak detection was at 377 nm. Biliverdin eluted at 12.4 min and Zn-biliverdin complex at 13.3 min. On-line HPLC/ESI-MS was done with the TFA-acetonitrile solvent system described above. The eluent from the HPLC column was split in the ratio of 9:1, allowing 100 μL/min of eluent to flow into the mass spectrometer. Data were acquired in the positive continuum mode at a rate of three spectra/s over the range m/z 100–1000 with the probe voltage set at 3.5 kV and a cone voltage of 30–90 V depending on the experiment. The source and desolvation temperature were set at 120 and 350 °C, respectively. Nitrogen desolvation and nebulizer gas flows were 350 and 50 L/h, respectively. Tandem MS/MS data were acquired at collision energy of 35 eV with argon as the collision gas. Product ions were acquired over the same range. To avoid carryover contamination, each sample run was followed by a blank run.

### Genomic DNA chip detection and sequencing–based genotyping

DNA was extracted from blood samples ($n = 64$ LP–BBS, $n = 44$ LP–NBS) by using a medium-volume blood genomic DNA extraction kit (DP332, TIANGEN Biotech Co., Ltd., Beijing, China) and was sequenced using the OvineSNP50 Genotyping BeadChip (WG-420, Illumina, San Diego, USA). Genotyped SNP data were combined with the downloaded data from ISGC, followed by quality control and to assess the LP–BBS population structures.

DNA was extracted from the same cohort of LP–BBS ($n = 64$) and LP–NBS ($n = 44$), and gene variants were validated through Sanger sequencing.

### Next-Generation sequencing (NGS) and variant identification

DNA was extracted from the blood of LP–BBS ($n = 16$) and LP–NBS ($n = 5$) individuals, and sequenced on the Illumina HiSeq 2000 platform with 10X and 30X coverage (Additional file 3: Table S10). After quality control, clean reads were aligned to the sheep genome reference sequence Oar_rambouillet_v1.0 (https://www.ncbi.nlm.nih.gov/assembly/GCF_002742125.1/) using the BWA MEM algorithm. SAMtools was used for alignment file format conversion. GATK v4 was applied to generate SNVs and Indels. Variant calling was conducted using HaplotypeCaller; the output of each sample was saved in GVCF format, and joint-calling was then done by GenotypeGVCFs with default parameters. The selectVariants tool filtered SNVs with Fisher Strand value > 60, QualbyDepth < 2, or Mapping Quality < 40, and filtered Indels with Fisher Strand > 200 or QualbyDepth < 2.

All SNVs segregated within the populations were extracted and pruned to remove pairs in LD with an $R^2$ correlation coefficient of 0.5 or greater. LD pruning and principal component decomposition calculations were carried out using PLINK v1.9, as mentioned in the PCA of the chip genotyped SNP data. The relatedness of all samples was inferred based on pairwise SNP data comparisons. To identify genetic sequences shared between individuals, haplotypes were resolved using BEAGLE v.4.

To investigate differences in genetic diversity and selection between LP–BBS and LP–NBS, we conducted a comparative analysis of mutations at functional loci based on VEP annotation categories. The relative excess of missense variants and deficit of LOF variants in LP–BBS was 2% higher than in LP–NBS. The fractions of variant types across the genome were similar in both LP–BBS and LP–NBS. Whole-genome expression data were subjected to gene set enrichment analysis (GSEA). Genome-wide distributions of $F_{ST}$ and θπ between LP–BBS and LP–NBS were calculated using a sliding-window approach (100-kb windows with 50-kb increments). $F_{ST}$ values were Z-transformed, and the θπ ratios were log2-transformed. Windows with top 5% $Z(F_{ST})$ and $\log_2(\theta\pi$ ratio) values were flagged as candidate selective sweeps. Outlier windows were mapped to corresponding SNPs and genes. A sliding-window strategy was also applied to calculate nucleotide diversity (π) and Tajima's D. Genes in selected regions were annotated and analyzed to elucidate genetic characteristics.

Genome Wide Association Study (GWAS) was conducted in a crossbred population ($n = 42$) from male LP-BBS ($n = 3$) and female Suffolk sheep ($n = 42$) using xpEHH to detect selective sweeps.

To further screen for additional variations in the FRRS1L gene, Sanger sequencing was conducted using pooled DNA extracted from blood samples of two cohorts: LP–BBS sheep ($n = 20$, including 16 samples from NGS and 4 from Shangri-La) and LP–NBS sheep ($n = 5$, all from NGS).

### RNA sequencing (RNA-seq) and data analysis

Total RNA was extracted from the spleen, liver, and kidney of LP–BBS ($n = 4$) and LP–NBS ($n = 4$) (Lanping county) using TRIZOL® Reagent (15596026, ThermoFisher Technology Co., Ltd., Shanghai, China). Libraries were sequenced on an Illumina Hiseq 2500 platform, and 100-bp paired-end reads were generated. Clean reads were generated after trimming by Trimmomatic and aligned to the reference genome using STAR. Gene expression values were normalized as fragments per kilobase of transcript per million mapped reads (FPKM). A gene was considered expressed only when its FPKM value was greater than zero in all three biological replicates. Differentially expressed genes were identified with thresholds of false discovery rate (FDR) < 0.05, fold change > 2, or fold change < 0.5 using the DESeq software package (bioconductor.org/).

### Quantitative RT-PCR (qPCR)

Total RNA (0.5 μg) extracted from the spleen, liver, kidney, and lymph node ($n = 5$ for both LP–BBS and LP–NBS groups), as described above, was transcribed into cDNA using the PrimeScript RT reagent Kit (KR118, TIANGEN Biotech Co., Ltd., Beijing, China). Primers were designed using Primer Premier 6.25 (Premier Biosoft, San Francisco, CA, USA) and synthesized by Sangon Biotech Co., Ltd. (Beijing, China). Gene expression levels were quantified using SYBR Green Real-time PCR Master Mix (FP205, TIANGEN Biotech Co., Ltd., Beijing, China). Data were collected from three biological replicates, with each biological replicate run in three technical replicates.

### Immunohistochemistry

To distinguish the expression of FRRS1L and determine if the pigment was located in macrophages, frozen sections of kidney, lung, and lymph node ($n = 5$ for both LP–BBS and LP–NBS) were washed with distilled water and treated with 3% hydrogen peroxide for 15 min at room temperature. After washing with PBS, the sections were treated with goat serum at room temperature for 30 min, then incubated with primary mouse anti-FRRS1L (1:200, sc-398692, Santa Cruz Biotechnology Co., Ltd., Shanghai, China) and anti-macrophage (1:500, ab58822, Abcam Biotechnology Co., Ltd., Shanghai, China) monoclonal antibodies at 4 °C overnight. After being washed three times in PBS, the sections were stained with HRP-conjugated goat anti-mouse antibody (1:200, ab6728, Abcam Biotechnology Co., Ltd., Shanghai, China) for 2 h at room temperature. Following three PBS washes, the sections were visualized with diaminobenzidine staining (Solarbio Technology Co., Ltd., Beijing, China) for 10 min at room temperature. After counterstaining with haematoxylin (Solarbio Technology Co., Ltd., Beijing, China), the sections were dehydrated and mounted with neutral balsam. FRRS1L expressions in tissues of LP–BBS and LP–NBS were quantified using Image–Pro Plus 9.0 based on integrated optical density (IOD) under the microscope magnifying 200x. For each sample, 10 random sites were analyzed for IOD by a single investigator to minimize bias.

### Double luciferase reporting assay

A chemical synthesis method was used to construct mutated vectors (Generay Biotech Co., Ltd., Shanghai, China). Six mutated fragments of the 3′-UTR (3′-untranslated region) of FRRS1L were cloned using Taq DNA polymerase and ligated into the psiCHECK2 vector (Promega Biotech Co., Ltd., Beijing, China) per the manufacturer's guidelines. After sequence confirmation, the constructed plasmids were transfected into DH5α (D1031S, Beyotime Biotechnology, Shanghai, China) for 12 h, then extracted using the plasmid midi kit (DP118, TIANGEN Biotech Co., Ltd., Beijing, China) according to the manufacturer′s instructions. The constructed plasmids were dissolved in sterile double-distilled water into a storage solution at 100 ng/μL. HEK 293T cells with high transfection efficiency were cultured in DMEM (Dulbecco′s Modified Eagle Medium) supplemented with 10% fetal bovine serum and 1% penicillin–streptomycin. All cell culture reagents were purchased from Thermo Fisher Technology Co., Ltd. (Shanghai, China). Cells were seeded into 24-cell plates (Corning, NY, USA) and transfected with 200 ng psiCHECK2-construction vector using Lipofectamine 2000 (11668027, ThermoFisher Technology Co., Ltd., Shanghai, China). Each construct included six biological replicates, with the psiCHECK2 vector and pRL-SV40 (E2231, Promega Biotech Co., Ltd., Beijing, China) as a blank control. After 36 h, firefly and renilla luciferase activities were measured using the Dual-Glo Luciferase Assay System (E2920, Promega Biotech Co., Ltd., Beijing, China). Relative luciferase activity was calculated by dividing the firefly luciferase signal by the renilla luciferase signal to normalize transfection efficiency. Significant differences were determined by a paired two-sided Student′s *t*-test.

### Cell culture and in vitro RNAi assay

Healthy Hu sheep aged one year ($n = 3$) were obtained from the animal farm of China Agricultural University, Beijing. The sera tested negative for brucellosis, infectious pleural pneumonia, streptococcus, and chlamydia. After euthanasia, the trachea was ligated, and the trachea and lung were isolated to dissociate primary cells. Sterile PBS was injected into the lungs via the trachea, and the collected PBS was centrifuged at 2500 r/min for 5 min. The cell pellets were resuspended and washed with 1x PBS. After three washes, the pellet was resuspended with red blood cell lysis buffer (R1010, Solarbio Technology Co., Ltd., Beijing, China) to remove red blood cells; after centrifugation, the pellet was resuspended and washed twice with RPMI1640 medium (22400071, ThermoFisher Technology Co., Ltd., Shanghai, China). Macrophages were cultured in modified RPMI1640 medium supplemented with 10% FBS (10100147, ThermoFisher Technology Co., Ltd., Shanghai, China) and 200 IU penicillin-streptomycin (10378016, ThermoFisher Technology Co., Ltd., Shanghai, China) for subsequent assays.

Macrophages were cultured in six-well plates with three biological replicates per group. After removing the cell culture supernatant, a hemin suspension prepared with fresh RPMI1640 medium was added to the cell culture wells, followed by continued incubation for 12 and 24 h. Total RNA was extracted from the hemin treated ($n = 3$) and blank ($n = 3$) macrophages using TRIZOL® Reagent (15596026, ThermoFisher Technology Co., Ltd., Shanghai, China), and performed RNA-sequencing (Shanghai OE Biomedical Technology Co., Ltd., Shanghai, China) to analyse their differentially expressed genes.

Macrophages (with or without *FRRS1* and *FRRS1L* siRNA interference) were cultured in six-well plates with three biological replicates per group. At 24 and 48 h post-transfection, macrophages were collected for total RNA extraction and qPCR. Total RNA was extracted using TRIZOL® Reagent (15596026, ThermoFisher Technology Co., Ltd., Shanghai, China) per the manufacturer's instructions. RNA (0.5 μg) was transcribed into cDNA using the FastQuant RT Kit (with gDNase) (KR118, TIANGEN Biotech Co., Ltd., Beijing, China). Gene expression levels were quantified by qPCR using SYBR Green Real-Time PCR Master Mix (FP205, TIANGEN

Biotech Co., Ltd., Beijing, China). Primers were designed eith Primer Premier 6.25 (Premier Biosoft, San Francisco, CA, USA) and synthesized by Sangon Biotech Co., Ltd. (Beijing, China). Cycling parameters: 95 °C for 4 min (initial denaturation); 40 cycles of 95 °C for 30 s, 59 °C for 30 s, and 72 °C for 30 s; and final extension at 72 °C for 5 min. Melting curve analysis was performed to confirm primer specificity and excluded genomic DNA contamination. Gene expression was normalized using the $2^{-\triangle\triangle CT}$ method with the glyceraldehyde 3-phosphate dehydrogenase (*GAPDH*) gene as an internal control. Each biologic duplicate was run in three technical replicates.

At 24 and 48 h post-transfection, macrophages were collected and digested with 0.25% trypsin-EDTA (25200072, ThermoFisher Technology Co., Ltd., Shanghai, China). After three centrifugation steps, homogenates were filtered through a cell strainer and centrifuged at 12,000 r/min for 10 min to collect crude pigment. The pigment was sequentially suspended in diethyl ether, ethyl alcohol, and deionized water; tubes were vortex-mixed for 1.5 min and centrifuged at 12,000 r/min for 2 min. Pigment was dissolved in tris-saturated phenol and analyzed by HPLC.

### Statistical analysis

Statistical analyses were performed using GraphPad Prism 9.0 (Graphpad Software, v9.1.1). Statistical analyses were performed using GraphPad Prism 9.0 (Graphpad Software, v9.1.1). Data are presented as mean ± standard error of mean (SEM). For cell culture, in vitro RNAi assays, and the double luciferase reporting assays, a paired, two-sided Student's *t*-test analysis was used. An unpaired, two-sided Student's *t*-test analysis was applied to all other experiments, e.g., comparisons between LP–BBS) and LP–NBS, due to the absence of pairwise matching. Results were considered significant at $p \leq 0.05$ (*), ≤ 0.01 (**), ≤ 0.001 (***), ≤ 0.0001 (****), and not significant (n.s.) when $p > 0.05$.

#### Abbreviations

| | |
|---|---|
| LP–BBS | Lanping–black bone sheep |
| LP–NBS | Lanping non-black bone sheep |
| HDMs | Hengduan Mountains |
| NL | Ninglang sheep |
| TC | Tengchong sheep |
| TIB | Tibetan sheep |
| AD | Anduo |
| CHA | Changtang |
| UJI | Ujimqin |
| NGS | Next generation sequencing |
| RNA-seq | RNA sequencing |
| qPCR | Quantitative polymerase Chain Reaction |
| 3′-UTR | 3′-untranslated region |
| SNPs | Single nucleotide polymorphisms |
| PCA | Principal component analysis |
| LD | Linkage disequilibrium |
| VEP | Variant Effect predictor |
| GO | Gene ontology |
| ROH | Runs of homo/autozygosity |
| GSEA | Gene set enrichment analysis |
| FPKM | Fragments per kilobase of transcript per million mapped reads |
| FDR | False-discovery rate |
| IOD | Integrated optical density |
| HPLC | High–performance liquid chromatography |
| HPLC-MS | HPLC-mass spectrometry |
| DEGs | Differentially expressed genes |
| GWAS | Genome-wide association studies |
| GSH-PX | Glutathione peroxidase |
| MDA | Malondialdehyde |

## Supplementary Information

The online version contains supplementary material available at https://doi.org/10.1186/s13578-025-01426-6.

Supplementary Material 1

Supplementary Material 2

Supplementary Material 3

#### Acknowledgements

We thank Mr. Duojie Sinan (Shangri-La Duojie Biological Resources Protection and Development Co. Ltd) for kindly providing part of blood samples of LP–BBS and LP–NBS. We thank Miss. Tianjiao Liu (College of Veterinary Medicine, China Agricultural University) for scientifically depicting visualization of heme metabolism and transport (Additional file 1: Figure S9).

#### Author contributions

XD, DH, and YZ conceived and designed the experiments. XD, DH, YZ, XY, YM, KC, HYAD, XD, JW, ZY, WD, HM and XG collected the corresponding sheep samples. DH and YZ prepared the DNA samples. YZ performed the SNP Beadchip data and whole genome sequencing data analysis. DH, YZ and GH prepared the RNA and analyzed the RNA sequencing data. DH, GH and JC performed qPCR analysis. DH, XY, GH, JC, YT and YY performed the histology, pigment extraction, and HPLC–MS detection. DH, XY, KC, GH, YM and YT collected the sheep alveolar macrophages. DH, JC, YT and G H performed double luciferase reporting assay, RNA interference and qPCR in vitro experiment. XD, WL, DH, SC and YZ performed the data visualization. DH, YZ, WL and XD wrote and revised the manuscript.

#### Funding

The research was supported by the grants from STI 2030-Major Projects (2023ZD040750X), the National Natural Science Foundation of China (U1136605), and the 2115 Talent Development program of China Agricultural University.

#### Data availability

All data generated or analyzed during this study are included in this published article, its supplementary information files, and publicly available repositories.

## Declarations

#### Ethics approval and consent to participate

The study was approved by the Animal Ethics Committee of China Agricultural University (approval number 201206078) and was performed in accordance to Regulations of Experimental Animals of Beijing Authority. Experimental protocols conformed to the guidelines of the Beijing Laboratory Animal Welfare and Ethics Committee and were approved by the Beijing Association for Science and Technology (approval number SYXK-2012-04-07).

#### Consent for publication

Not applicable.

#### Competing interests

The authors declare that they have no competing interests.

**Author details**
[1]Animal Genetics, Breeding, and Reproduction of the Ministry of Agriculture, Beijing Key Laboratory for Animal Genetic Improvement, State Key Laboratory of Animal Biotech Breeding, China Agricultural University, Beijing 100193, China
[2]Laboratory of Advanced Agricultural Sciences in Weifang, Peking University Institute of Advanced Agricultural Sciences, Weifang City 261325, Shandong, China
[3]Department of Animal Science, Center for Reproductive Biology and Health, College of Agricultural Sciences, The Pennsylvania State University, University Park 16802, PA, USA
[4]Faculty of Animal Science and Technology, Yunnan Agricultural University, Kunming 650201, China
[5]Beijing University of Agriculture, Animal Science and Technology College, Beijing 100096, China

Received: 7 January 2025 / Accepted: 6 June 2025
Published online: 24 June 2025

**References**

1. Lin JY, Fisher DE. 2007. Melanocyte biology and skin pigmentation. *Nature* 445:843–850. https://doi.org/10.1038/nature05660. PMID: 17314970.
2. Wiemann J, Yang TR, Norell MA. 2018. Dinosaur egg colour had a single evolutionary origin. *Nature* 563:555–558. https://doi.org/10.1038/s41586-018-0646-5. PMID: 30464264.
3. Chen JJ, Zhang S. 2019. Heme-regulated eIF2alpha kinase in erythropoiesis and hemoglobinopathies. *Blood* 134:1697–1707. https://doi.org/10.1182/blood.2019001915. PMID: 31554636.
4. Grace RF, Barcellini W. 2020. Management of pyruvate kinase deficiency in children and adults. *Blood* 136:1241–1249. https://doi.org/10.1182/blood.2019000945. PMID: 32702739.
5. Joly BS, Coppo P, Veyradier A. 2017. Thrombotic thrombocytopenic purpura. *Blood* 129:2836–2846. doi: 10.1080/17474086.2019.1611423. PMID: 31107120.
6. Menon AV, Liu J, Tsai HP, Zeng L, Yang S, Asnani A, Kim J. 2022. Excess heme upregulates heme oxygenase 1 and promotes cardiac ferroptosis in mice with sickle cell disease. *Blood* 139:936–941. https://doi.org/10.1182/blood.2020008455. PMID: 34388243.
7. Beaumont C, Leneuve P, Devaux I, Scoazec JY, Berthier M, Loiseau MN, Grandchamp B, Bonneau D. 1995. Mutation in the iron responsive element of the L ferritin mRNA in a family with dominant hyperferritinaemia and cataract. *Nature Genetics* 11:444–446. https://doi.org/10.1038/ng1295-444. PMID: 7493028.
8. Awandare GA, Kempaiah P, Ochiel DO, Piazza P, Keller CC, Perkins DJ. 2011. Mechanisms of erythropoiesis inhibition by malarial pigment and malaria-induced proinflammatory mediators in an in vitro model. *American Journal of Hematology*. 86:155–162. https://doi.org/10.1002/ajh.21933. PMID: 21264897.
9. Granstein RD, Sober AJ. 1981. Drug- and heavy metal–induced hyperpigmentation. *Journal of the American Academy of Dermatology* 5:1–18. https://doi.org/10.1016/s0190-9622(81)70072-0. PMID: 6268671.
10. Fernandez-Flores A, Nguyen T, Cassarino DS. 2017. Mucocutaneous Hyperpigmentation in a Patient With a History of Both Minocycline and Silver Ingestion. American *Journal of Dermatopathology* 39:916–919. https://doi.org/10.1097/DAD.0000000000000920. PMID: 28475520.
11. Dorshorst B, Molin AM, Rubin CJ, Johansson AM, Stromstedt L, Pham MH, Chen CF, Hallbook F, Ashwell C, Andersson L. 2011. A complex genomic rearrangement involving the endothelin 3 locus causes dermal hyperpigmentation in the chicken. *PLoS Genetics* 7:e1002412. https://doi.org/10.1371/journal.pgen.1002412. PMID: 22216010.
12. Shinomiya A, Kayashima Y, Kinoshita K, Mizutani M, Namikawa T, Matsuda Y, Akiyama T. 2012. Gene duplication of endothelin 3 is closely correlated with the hyperpigmentation of the internal organs (Fibromelanosis) in silky chickens. *Genetics* 190:627–638. https://doi.org/10.1534/genetics.111.136705. PMID: 22135351.
13. Deng WD, Yang SL, Huo YQ, Gou X, Shi XW, Mao HM. 2006. Physiological and genetic characteristics of black-boned sheep (Ovis aries). *Animal Genetics* 37:586–588. https://doi.org/10.1111/j.1365-2052.2006.01530.x. PMID: 17121605.
14. Chen D, Wang SS, Zou Y, Li Z, Xie SC, Shi LQ, Zou FC, Zhu XQ, Yang JF, Zhao GH. 2018. Prevalence and multi-locus genotypes of Enterocytozoon bieneusi in black-boned sheep and goats in Yunnan Province, southwestern China. *Infection, Genetics and Evolution* 65:385–391. https://doi.org/10.1016/j.meegid.2018.08.022. MID: 30145389.
15. Xing Y, Ree RH. 2017. Uplift-driven diversification in the Hengduan Mountains, a temperate biodiversity hotspot. *PNAS* 114:E3444-E3451. https://doi.org/10.1073/pnas.1616063114. PMID: 28373546.
16. Hsu CC, Senussi NH, Fertrin KY, Kowdley KV. 2022. Iron overload disorders. *Hepatology Communications* 6:1842–1854. https://doi.org/10.1002/hep4.2012. PMID: 35699322.
17. Brissot P, Pietrangelo A, Adams PC, de Graaff B, McLaren CE, Loréal O. 2018. Haemochromatosis. *Nature Reviews Disease Primers* 4:18016. https://doi.org/10.1038/nrdp.2018.16. PMID: 29620054.
18. Mattman A, Huntsman D, Lockitch G, Langlois S, Buskard N, Ralston D, Butterfield Y, Rodrigues P, Jones S, Porto G, Marra M, De Sousa M, Vatcher G. 2002. Transferrin receptor 2 (TfR2) and HFE mutational analysis in nonC282Y iron overload: identification of a novel TfR2 mutation. *Blood* 100:1075-7. https://doi.org/10.1182/blood-2002-01-0133. PMID: 12130528.
19. Papanikolaou G, Samuels ME, Ludwig EH, MacDonald ML, Franchini PL, Dubé MP, Andres L, MacFarlane J, Sakellaropoulos N, Politou M, Nemeth E, Thompson J, Risler JK, Zaborowska C, Babakaiff R, Radomski CC, Pape TD, Davidas O, Christakis J, Brissot P, Lockitch G, Ganz T, Hayden MR, Goldberg YP. 2004. Mutations in HFE2 cause iron overload in chromosome 1qlinked juvenile hemochromatosis. *Nature Genetics* 36:77–82. https://doi.org/10.1038/ng1274. PMID: 14647275.
20. Barton JC, Lafreniere SA, Leiendecker-Foster C, Li H, Acton RT, Press RD, Eckfeldt JH. 2009. HFE, SLC40A1, HAMP, HJV, TFR2, and FTL mutations detected by denaturing high-performance liquid chromatography after iron phenotyping and HFE C282Y and H63D genotyping in 785 HEIRS Study participants. *American Journal of Hematology* 84:710–714.https://doi.org/10.1002/ajh.21524. PMID: 19787796.
21. Del-Castillo-Rueda A, Moreno-Carralero MI, Cuadrado-Grande N, Alvarez-Sala-Walther LA, Enríquez-de-Salamanca R, Méndez M, Morán-Jiménez MJ. 2012. Mutations in the HFE, TFR2, and SLC40A1 genes in patients with hemochromatosis. *Gene* 508:15–20. https://doi.org/10.1016/j.gene.2012.07.069. PMID: 22890139.
22. Kowdley KV, Brown KE, Ahn J, Sundaram V. 2019. ACG Clinical Guideline: Hereditary Hemochromatosis. *American Journal of Gastroenterology* 114:1202–1218. https://doi.org/10.14309/ajg.0000000000000315. PMID: 31335359.
23. Norris BJ, Whan VA. 2008. A gene duplication affecting expression of the ovine ASIP gene is responsible for white and black sheep. *Genome Research* 18:1282–1293. https://doi.org/10.1101/gr.072090.107. PMID: 18493018.
24. Deng WD, Xi DM, Gou X, Yang SL, Shi XW, Mao HM. 2008. Pigmentation in Black-boned sheep (Ovis aries): association with polymorphism of the Tyrosinase gene. *Molecular Biology Reports* 35:379–385. https://doi.org/10.1007/s11033-007-9097-z. PMID: 17520341.
25. Deng W, Tan Y, Wang X, Xi D, He Y, Yang S, Mao H, Gao S. 2009. Molecular cloning, sequence characteristics, and polymorphism analyses of the tyrosinase-related protein 2 / DOPAchrome tautomerase gene of black-boned sheep (Ovis aries). *Genome* 52:1001–1011. https://doi.org/10.1139/G09-078. PMID: 19953128.
26. Deng WD, Shu W, Yang SL, Shi XW, Mao HM. 2009. Pigmentation in Black-boned sheep (Ovis aries): association with polymorphism of the MC1R gene. *Molecular Biology Reports* 36:431–436. https://doi.org/10.1007/s11033-007-9197-9. PMID: 18075782.
27. Darwish HYA, Zhang Y, Cui K, Yang Z, Han D, Dong X, Mao H, Deng W, Deng X. 2018. Molecular cloning and characterization of the endothelin 3 gene in black bone sheep. *Journal of Animal Science and Biotechnology* 9:57. https://doi.org/10.1186/s40104-018-0272-y. eCollection 2018. PMID: 29988351.
28. Adams PC, Jeffrey G, Ryan J. 2023. Haemochromatosis. *Lancet* 401:1811–1821. https://doi.org/10.1016/S0140-6736(23)00287-8. PMID: 37121243.
29. Bowes O, Baxter K, Elsey T, Snead M, Cox T. 2014. Hereditary hyperferritinaemia cataract syndrome. *Lancet* 383:1520. https://doi.org/10.1016/S0140-6736(14)60484-0. PMID: 24766965.
30. Franchini M. 2006. Hereditary iron overload: update on pathophysiology, diagnosis, and treatment. *American Journal of Hematology* 81:202–209. https://doi.org/10.1002/ajh.20493. PMID: 16493621.
31. Rouault TA. 2013. Iron metabolism in the CNS: implications for neurodegenerative diseases. *Nature Reviews Neuroscience* 14:551–564. https://doi.org/10.1038/nrn3453. PMID: 23820773.
32. Pietrangelo A, Haemochromatosis. *Gut* 52 Suppl 2(Suppl 2):ii23-30. https://doi.org/10.1136/gut.52.suppl_2.ii23. PMID: 12651879.

33. Pietrangelo A. 2010. Hereditary hemochromatosis: pathogenesis, diagnosis, and treatment. *Gastroenterology* 139:393–408, 408 e391-392. https://doi.org/10.1053/j.gastro.2010.06.013. PMID: 20542038.
34. Ward J, Motwani J, Baker N, Nash M, Ewer AK, Toldi G. 2019. Congenital Methemoglobinemia Identified by Pulse Oximetry Screening. *Pediatrics* 143:e20182814. https://doi.org/10.1542/peds.2018-2814. PMID: 30733239.
35. Hayashi A, Wada Y, Suzuki T, Shimizu A. Studies on Familial hypotransferrinemia: unique clinical course and molecular pathology. Am J Hum Genet. 1993;53:201–13. PMID: 8317485.
36. Brechet A, Buchert R, Schwenk J, Boudkkazi S, Zolles G, Siquier-Pernet K, Schaber I, Bildl W, Saadi A, Bole-Feysot C, Nitschke P, Reis A, Sticht H, Al-Sanna'a N, Rolfs A, Kulik A, Schulte U, Colleaux L, Abou Jamra R, Fakler B. 2017. AMPA receptor specific biogenesis complexes control synaptic transmission and intellectual ability. *Nature Communication* 8: 15910. https://doi.org/10.1038/ncomms15910. PMID: 28675162.
37. Stewart M, Lau P, Banks G, Bains RS, Castroflorio E, Oliver PL, Dixon CL, Kruer MC, Kullmann DM, Acevedo-Arozena A, Wells SE, Corrochano S, Nolan PM. 2019. Loss of Frrs1l disrupts synaptic AMPA receptor function, and results in neurodevelopmental, motor, cognitive and electrographical abnormalities. *Disease Models & Mechanisms* 12:dmm036906. https://doi.org/10.1242/dmm.036806. PMID: 30692144.
38. Schwenk J, Boudkkazi S, Kocylowski MK, Brechet A, Zolles G, Bus T, Costa K, Kollewe A, Jordan J, Bank J, Bildl W, Sprengel R, Kulik A, Roeper J, Schulte U, Fakler B. 2019. An ER Assembly Line of AMPA-Receptors Controls Excitatory Neurotransmission and Its Plasticity. *Neuron* 104:680–692.e9. https://doi.org/10.1016/j.neuron.2019.08.033. PMID: 31604597.
39. Madeo M, Stewart M, Sun Y, Sahir N, Wiethoff S, Chandrasekar I, Yarrow A, Rosenfeld JA, Yang Y, Cordeiro D, McCormick EM, Muraresku CC, Jepperson TN, McBeth LJ, Seidahmed MZ, El Khashab HY, Hamad M, Azzedine H, Clark K, Corrochano S, Wells S, Elting MW, Weiss MM, Burn S, Myers A, Landsverk M, Crotwell PL, Waisfisz Q, Wolf NI, Nolan PM, Padilla-Lopez S, Houlden H, Lifton R, Mane S, Singh BB, Falk MJ, Mercimek-Mahmutoglu S, Bilguvar K, Salih MA, Acevedo-Arozena A, Kruer MC. 2016. Loss-of-Function Mutations in FRRS1L Lead to an Epileptic-Dyskinetic Encephalopathy. *American Journal of Human Genetics* 98:1249–1255. https://doi.org/10.1016/j.ajhg.2016.04.008. PMID: 27236917.
40. Han W, Wang H, Li J, Zhang S, Lu W. 2017. Ferric Chelate Reductase 1 Like Protein (FRRS1L) Associates with Dynein Vesicles and Regulates Glutamatergic Synaptic Transmission. *Frontiers in Molecular Neuroscience* 10:402. https://doi.org/10.3389/fnmol.2017.00402. eCollection 2017. PMID: 29276473.
41. Iyer LM, Anantharaman V, Aravind L. 2007. The DOMON domains are involved in heme and sugar recognition. *Bioinformatics* 23:2660–2664. https://doi.org/10.1093/bioinformatics/btm411. PMID: 17878204.
42. Orillard E, Anaya S, Johnson MS, Watts KJ. Oxygen-Induced conformational changes in the PAS-Heme domain of the Pseudomonas aeruginosa Aer2 receptor. Biochemistry. 2021;60:2610–22. https://doi.org/10.1021/acs.biochem.1c00452. PMID: 34383467.
43. Ding WN, Ree RH, Spicer RA, Xing YW. 2020. Ancient orogenic and monsoon-driven assembly of the world's richest temperate alpine flora. *Science* 369:578–581. https://doi.org/10.1126/science.abb4484. PMID: 32732426.
44. Li M, Tian S, Jin L, Zhou G, Li Y, Zhang Y, Wang T, Yeung CK, Chen L, Ma J, Zhang J, Jiang A, Li J, Zhou C, Zhang J, Liu Y, Sun X, Zhao H, Niu Z, Lou P, Xian L, Shen X, Liu S, Zhang S, Zhang M, Zhu L, Shuai S, Bai L, Tang G, Liu H, Jiang Y, Mai M, Xiao J, Wang X, Zhou Q, Wang Z, Stothard P, Xue M, Gao X, Luo Z, Gu Y, Zhu H, Hu X, Zhao Y, Plastow GS, Wang J, Jiang Z, Li K, Li N, Li X, Li R. 2013. Genomic analyses identify distinct patterns of selection in domesticated pigs and Tibetan wild boars. *Nature Genetics* 45:1431–1438. https://doi.org/10.1038/ng.2811. PMID: 24162736.
45. Gou X, Wang Z, Li N, Qiu F, Xu Z, Yan D, Yang S, Jia J, Kong X, Wei Z, Lu S, Lian L, Wu C, Wang X, Li G, Ma T, Jiang Q, Zhao X, Yang J, Liu B, Wei D, Li H, Yang J, Yan Y, Zhao G, Dong X, Li M, Deng W, Leng J, Wei C, Wang C, Mao H, Zhang H, Ding G, Li Y. 2014. Whole-genome sequencing of six dog breeds from continuous altitudes reveals adaptation to high-altitude hypoxia. *Genome Research* 24:1308–1315. https://doi.org/10.1101/gr.171876.113. PMID: 24721644.
46. Yu L, Wang GD, Ruan J, Chen YB, Yang CP, Cao X, Wu H, Liu YH, Du ZL, Wang XP, Yang J, Cheng SC, Zhong L, Wang L, Wang X, Hu JY, Fang L, Bai B, Wang KL, Yuan N, Wu SF, Li BG, Zhang JG, Yang YQ, Zhang CL, Long YC, Li HS, Yang JY, Irwin DM, Ryder OA, Li Y, Wu CI, Zhang YP. 2016. Genomic analysis of snub-nosed monkeys (Rhinopithecus) identifies genes and processes related to high-altitude adaptation. *Nature Genetics* 48:947–952. https://doi.org/10.1038/ng.3615. PMID: 27399969.
47. Qiu Q, Zhang G, Ma T, Qian W, Wang J, Ye Z, Cao C, Hu Q, Kim J, Larkin DM, Auvil L, Capitanu B, Ma J, Lewin HA, Qian X, Lang Y, Zhou R, Wang L, Wang K, Xia J, Liao S, Pan S, Lu X, Hou H, Wang Y, Zang X, Yin Y, Ma H, Zhang J, Wang Z, Zhang Y, Zhang D, Yonezawa T, Hasegawa M, Zhong Y, Liu W, Zhang Y, Huang Z, Zhang S, Long R, Yang H, Wang J, Lenstra JA, Cooper DN, Wu Y, Wang J, Shi P, Wang J, Liu J. 2012. The yak genome and adaptation to life at high altitude. *Nature Genetics* 44:946–949. https://doi.org/10.1038/ng.2343. PMID: 22751099.
48. Lorenzo FR, Huff C, Myllymäki M, Olenchock B, Swierczek S, Tashi T, Gordeuk V, Wuren T, Ri-Li G, McClain DA, Khan TM, Koul PA, Guchhait P, Salama ME, Xing J, Semenza GL, Liberzon E, Wilson A, Simonson TS, Jorde LB, Kaelin WG Jr, Koivunen P, Prchal JT. 2014. A genetic mechanism for Tibetan high-altitude adaptation. *Nature Genetics* 46:951–956. https://doi.org/10.1038/ng.3067. PMID: 25129147.
49. Beall CM. 2020. Hemoglobin, altitude, and sensitive Swiss men. *Blood* 135:984–985. https://doi.org/10.1182/blood.2020005251. PMID: 32219350.
50. Olynyk JK, Ramm GA. 2022. Hemochromatosis. *New England Journal of Medicine* 387:2159–2170. https://doi.org/10.1056/NEJMra2119758. PMID: 36477033.


## Publisher's note